

## Review

# Graphitic Carbon Nitride-Based Composite in Advanced Oxidation Processes for Aqueous Organic Pollutants Removal: A Review

Yu Shen, Antonio J. Dos santos-García  and María José Martín de Vidales \*

Department of Mechanical, Chemical and Industrial Design Engineering, ETSIDI, Universidad Politécnica de Madrid (UPM), 28012 Madrid, Spain; yu.shen@alumnos.upm.es (Y.S.); aj.dossantos@upm.es (A.J.D.s.-G.)

\* Correspondence: mariajose.martindevidales@upm.es; Tel.: +34-91-067-7722

**Abstract:** In recent decades, a growing number of organic pollutants released have raised world-wide concern. Graphitic carbon nitride ( $g-C_3N_4$ ) has drawn increasing attention in environmental pollutants removal thanks to its unique electronic band structure and excellent physicochemical stability. This paper reviews the recent progress of  $g-C_3N_4$ -based composites as catalysts in various advanced oxidation processes (AOPs), including chemical, photochemical, and electrochemical AOPs. Strategies for enhancing catalytic performance such as element-doping, nanostructure design, and heterojunction construction are summarized in detail. The catalytic degradation mechanisms are also discussed briefly.

**Keywords:** graphitic carbon nitride; aqueous organic pollutants removal; advanced oxidation processes



**Citation:** Shen, Y.; Dos santos-García, A.J.; Martín de Vidales, M.J. Graphitic Carbon Nitride-Based Composite in Advanced Oxidation Processes for Aqueous Organic Pollutants Removal: A Review. *Processes* **2021**, *9*, 66. <https://doi.org/10.3390/pr9010066>

Received: 26 November 2020

Accepted: 27 December 2020

Published: 30 December 2020

**Publisher's Note:** MDPI stays neutral with regard to jurisdictional claims in published maps and institutional affiliations.



**Copyright:** © 2020 by the authors. Licensee MDPI, Basel, Switzerland. This article is an open access article distributed under the terms and conditions of the Creative Commons Attribution (CC BY) license (<https://creativecommons.org/licenses/by/4.0/>).

## 1. Introduction

In recent years, environmental pollution, especially water pollution, is increasingly becoming a major concern worldwide. Many organic pollutions, such as pharmaceuticals and personal care products (PPCPs), pesticides, and organic dyes are toxic and refractory [1–4]. Various techniques have been developed to eliminate aqueous organic pollutants (e.g., extraction, adsorption, biological treatment, and advanced oxidation processes) [5–9]. Advanced oxidation processes (AOPs) are regarded as effective techniques for organic contaminants removal from water and wastewater [10–14].

The AOPs utilize highly reactive species (mainly hydroxyl radical,  $\bullet OH$ ) to oxidize the organic pollutants into less toxic or no-toxic products such as  $CO_2$  and  $H_2O$  [15,16]. According to supplied energies and reactive species, AOPs can be categorized as photocatalysis, electrocatalysis, sonolysis, ozonation, Fenton/Fenton-like reactions, and sulfate radical-based AOPs (SR-AOPs), among others [17,18]. In recent decades, numerous studies have been conducted to develop novel AOPs. Emerging energy sources (e.g., ionizing radiation with electron beams and  $\gamma$ -radiolysis, pulsed plasma, etc.) were applied, and different reactive species (such as periodate or ferrate reagent) were introduced [19–22]. Considering the merits of different AOPs, combinations of various processes are more common approaches to enhance degradation efficiency [21]. Although some AOPs (e.g.,  $UV/H_2O_2$ ,  $UV$ /peroxymonosulfate (PMS)) work properly without catalysts, employing catalysts can significantly reduce energy and reagent (source of reactive species) consumption [23]. Therefore, designing an effective and stable catalyst is a crucial strategy for the development of AOPs.

Graphitic carbon nitride ( $g-C_3N_4$ ), known as a metal-free polymer semiconductor, has attracted increasing attention due to its unique electronic band structure, anti-photocorrosion, excellent physicochemical stability, and easy availability [24,25]. The bandgap of  $g-C_3N_4$  is about 2.7 eV, which enables it to absorb all viewing range of solar irradiation. The valance band (VB) and conduction band (CB) mainly encompass nitrogen and carbon  $p_z$  orbitals

while VB top and CB bottom are located at about +1.4 and −1.3 eV, respectively [26–28]. The study of g-C<sub>3</sub>N<sub>4</sub> can be traced back to 1834, when Berzelius first synthesized a polymeric derivative of g-C<sub>3</sub>N<sub>4</sub>, and Liebig named it melon [29]. In 2006, Goettmann and his co-workers investigated Friedel–Crafts reactions that can be catalyzed by g-C<sub>3</sub>N<sub>4</sub>, which is its first application in the catalytic field [30]. In 2009, g-C<sub>3</sub>N<sub>4</sub> was demonstrated as a good metal-free photocatalyst for water splitting by Wang et al. [26]. Up to now, g-C<sub>3</sub>N<sub>4</sub> has been in-depth studied and extensively applied in photocatalysis. The g-C<sub>3</sub>N<sub>4</sub> preparation relies on (solvo)thermal polymerization of nitrogen-rich precursors such as melamine, dicyandiamide, and urea [31]. In addition, hard/soft template-assisted methods and sol-gel methods are frequently used to modify the synthesis approaches. The reaction parameters such as precursors and temperature could significantly affect the physicochemical property, including specific surface area, bandgap, etc. [32]. However, the pure g-C<sub>3</sub>N<sub>4</sub> encounters several drawbacks, including tiny surface area, inefficient use of visible light, low electric conductivity, and fast recombination of photo-induced carriers, which are not beneficial to its catalytic activity [33,34]. To address these issues, a lot of efforts such as (1) engineering the nanostructure of g-C<sub>3</sub>N<sub>4</sub> [27,35–37], (2) introducing heteroatoms (metals [38–44] or non-metals [45–50]), (3) coupling with other semiconductors [51–57] and (4) co-polymerization [58–61] were made. g-C<sub>3</sub>N<sub>4</sub> based composites hold unique advantages for organic pollutants removal from groundwater and wastewater due to the good adsorption capacity of g-C<sub>3</sub>N<sub>4</sub> for organic molecules, which could be attributed to strong intermolecular forces like hydrogen bonding,  $\pi$ - $\pi$  interactions between pollutant molecules and residual amino groups in the g-C<sub>3</sub>N<sub>4</sub> fragment [62,63]. On the other hand, introducing extra sources of reactive species such as H<sub>2</sub>O<sub>2</sub> or PMS in photocatalysis can significantly increase degradation efficiency [64,65]. Furthermore, some studies have explored g-C<sub>3</sub>N<sub>4</sub> based composites for organic pollutants removal without light irradiation in the presence of PMS or H<sub>2</sub>O<sub>2</sub> [66–69].

Some excellent reviews on g-C<sub>3</sub>N<sub>4</sub> based composites involving pollution remediation have been published [25,31,70,71]. g-C<sub>3</sub>N<sub>4</sub> based composites as photocatalysts for water purification have been summarized in these reviews, while no reviews involve other AOPs such as chemical AOPs and electrochemical AOPs. The dramatically increasing amounts of g-C<sub>3</sub>N<sub>4</sub> based composites in the range of AOPs fields requires a broader, thorough, and up-date assessment. This review is mainly focused on the application of g-C<sub>3</sub>N<sub>4</sub> based composites in chemical AOPs and electrochemical AOPs. The challenge and strategies for enhancing photodegradation performance using g-C<sub>3</sub>N<sub>4</sub> based composites as photocatalyst were also included.

## 2. Chemical AOPs

The chemical AOPs started as early as the application of the Fenton reaction to water treatment, in which •OH can be generated from the catalytic decomposition of H<sub>2</sub>O<sub>2</sub> by Fe<sup>2+</sup> for the destruction of various organic pollutants (Equation (1)) [10].



With the increasing demand for water treatment, various oxidants such as O<sub>3</sub>, PMS, peroxydisulfate (PDS) were applied in chemical AOPs. The PMS and PDS could be heterogeneous activated, and reactive species such as •SO<sub>4</sub><sup>−</sup> are subsequently generated to degrade organic pollutants [72–74]. Table 1 summarizes the part of a representative study using g-C<sub>3</sub>N<sub>4</sub> based composites as a catalyst in chemical AOPs.

**Table 1.** Graphitic carbon nitride (g-C<sub>3</sub>N<sub>4</sub>) based composites for chemical advanced oxidation processes (AOPs).

Catalyst	Target Contaminants	Oxidant	Reaction Conditions	Performance	Ref.
Cu(II)/CuAlO <sub>2</sub> /g-C <sub>3</sub> N <sub>4</sub>	Bisphenol A (BPA)	H <sub>2</sub> O <sub>2</sub>	BPA, 25 mg/L; catalyst, 1 g/L; H <sub>2</sub> O <sub>2</sub> , 10 mM; T, 35 °C; pH, 7	95.5% in 120 min	[75]
Cu/Al <sub>2</sub> O <sub>3</sub> /g-C <sub>3</sub> N <sub>4</sub>	Rhodamine B (RhB)	H <sub>2</sub> O <sub>2</sub>	RhB, 20 mg/L; catalyst, 1 g/L; H <sub>2</sub> O <sub>2</sub> , 10 mM; T, 25 °C; pH, 4.9	96.4% in 100 min	[76]
Iron oxide/g-C <sub>3</sub> N <sub>4</sub>	Ciprofloxacin	H <sub>2</sub> O <sub>2</sub>	ciprofloxacin, 20 mg/L; catalyst, 1 g/L; H <sub>2</sub> O <sub>2</sub> , 5.6 mM; pH, 3	100% in 60 min	[68]
g-C <sub>3</sub> N <sub>4</sub> /carbon nanotubes/Fe(II)	Methylene blue	H <sub>2</sub> O <sub>2</sub>	Methylene Blue, 90 mg/L; catalyst, 0.5 g/L; H <sub>2</sub> O <sub>2</sub> , 1 mM; T, 25 °C; pH, 4.9	66.8% in 1 h	[69]
Fe <sub>3</sub> O <sub>4</sub> @C/g-C <sub>3</sub> N <sub>4</sub>	Acid orange 7 (AO 7)	PMS	AO 7, 20 mg/L; catalyst, 0.6 g/L; PMS, 0.1 g/L; T, 25 °C; pH, 4	97% in 20 min	[77]
CoFeO <sub>2</sub> /g-C <sub>3</sub> N <sub>4</sub>	Levofloxacin	PMS	levofloxacin, 10 mg/L; catalyst, 0.15 g/L; PMS, 0.5 mM; T, Room temperature; pH, 3	100% in 60 min	[78]
Co-doped g-C <sub>3</sub> N <sub>4</sub>	4-chlorophenol	PMS	4-chlorophenol, 50 mg/L; catalyst, 1 g/L; PMS, 2.5 mM	100% in 30 min	[79]
Mn-doped g-C <sub>3</sub> N <sub>4</sub>	Acetaminophen	PMS	acetaminophen, 20 mg/L; catalyst, 0.05 g/L; PMS, 0.8 g/L; pH, 6.5	100% in 15 min	[80]
Cu <sup>+</sup> -g-C <sub>3</sub> N <sub>4</sub>	Rhodamine B	H <sub>2</sub> O <sub>2</sub>	Rhodamine B, 50 mg/L; catalyst, 0.8 g/L; H <sub>2</sub> O <sub>2</sub> , 40 mM; pH, neutral	99.2% in 1 h	[81]
Pd/g-C <sub>3</sub> N <sub>4</sub>	BPA	PMS	BPA, 20 mg/L; catalyst, 0.1 g/L; PMS, 1 mM; T, 25 °C; pH, 9	91% in 60 min	[82]
FeO <sub>y</sub> /S-g-C <sub>3</sub> N <sub>4</sub>	Sulfamethoxazole	PMS	sulfamethoxazole, 10 mg/L; catalyst, 0.5 g/L; PMS, 0.8 mM; T, 25 °C; pH, 3.54	100% in 60 min	[83]
Fe(III)-doped g-C <sub>3</sub> N <sub>4</sub>	AO 7	PMS	AO 7, 8.5 mg/L; catalyst, 0.1 g/L; PMS, 0.1 g/L; pH, 3–4	97% in 30 min	[84]
cryptomelane-type manganese oxide/g-C <sub>3</sub> N <sub>4</sub>	AO 7	PMS	AO 7, 0.13 mM; catalyst, 0.2 g/L; PMS, 0.65 mM; T, 8 °C; pH, 7.25	88% in 30 min	[85]
carbon and oxygen dual-doped g-C <sub>3</sub> N <sub>4</sub>	BPA	PMS	BPA, 0.1 mM; catalyst, 0.5 g/L; PMS, 5 mM; T, 30 °C; pH, 6.7	100% in 60 min	[86]
Active carbon/g-C <sub>3</sub> N <sub>4</sub>	AO 7	PMS	AO 7, 50 mg/L; catalyst, 0.2 g/L; PMS, 0.4 g/L; T, 27 °C; pH, 3.82	100% in 20 min	[87]
Fe-doped g-C <sub>3</sub> N <sub>4</sub> /graphite	4-chlorophenol	PMS	4-chlorophenol, 0.1 mM; catalyst, 0.1 g/L; PMS, 0.1 mM; pH, 3	100% in 10 min	[88]
Oxygen-doped g-C <sub>3</sub> N <sub>4</sub>	BPA	PMS	BPA, 0.05 mM; catalyst, 1 g/L; PMS, 10 mM; T, 30 °C; pH, 3–9	100% in 60 min	[66]
Fe(II)-doped g-C <sub>3</sub> N <sub>4</sub>	Phenol	PMS	phenol, 0.1 mM; catalyst, 1 g/L; PMS, 5 mM; T, 23 °C; pH, 2.6	100% in 20 min	[89]
Mn <sub>3</sub> O <sub>4</sub> /g-C <sub>3</sub> N <sub>4</sub>	4-chlorophenol	PMS	4-chlorophenol, 50 mg/L; catalyst, 0.3 g/L; PMS, 1 mM; T, 25 °C; pH, 4	100% in 40 min	[90]

Pure g-C<sub>3</sub>N<sub>4</sub> holds inert activation performance of oxidants such as H<sub>2</sub>O<sub>2</sub> and PMS. Considering that g-C<sub>3</sub>N<sub>4</sub> has excellent affinity to entrap transition metal ions, metal doping is the main strategy for improving the catalytic activity. Oh et al. investigated the catalytic activities of Me-doped g-C<sub>3</sub>N<sub>4</sub> (Me = Cu, Co, and Fe) as PMS activator for sulfathiazole degradation. Among the prepared catalyst, Co-doped g-C<sub>3</sub>N<sub>4</sub> (0.59 wt% Co) exhibited the highest degradation efficiency for sulfathiazole, while excessive metal

doping and surface defects ( $-\text{C}\equiv\text{N}$ ) had a scavenging effect for  $\bullet\text{SO}_4^-$  [91]. The authors further studied Fe-doped  $\text{g-C}_3\text{N}_4$  for acid orange 7 degradation, and the non-radical pathway was proposed [84]. Li et al. prepared Fe doped  $\text{g-C}_3\text{N}_4$  as PMS activator for phenolic compounds degradation.  $(\text{Fe(V)}=\text{O})$  generated from the oxidation of  $\text{Fe(III)-N}$  was proposed as dominant reactive species [67]. In another work, Fe doped  $\text{g-C}_3\text{N}_4$  was also employed in PMS activation for phenol degradation. Authors investigated the ratio of 46% and 54% of Fe (III) and Fe (II) via Mössbauer spectra, while the XPS survey spectra suggested the primary Fe on the surface of the catalyst was in the 3+ state. It was proposed that the Fe (II) complex heterolyzed at the O-O bond of activated PMS to form  $\text{Fe(IV)}=\text{O}$ , which was the primary active species [89]. In PMS/Mn-doped  $\text{g-C}_3\text{N}_4$  system, superoxide radical was firstly generated due to the PMS bounding to the Mn-N site, and singlet oxygen produced by superoxide radical was proposed as the responsible reactive species for acetaminophen degradation [80]. Ma et al. synthesized Cu (I)-doped  $\text{g-C}_3\text{N}_4$  for the removal of rhodamine B in a Fenton-like reaction. Cu (I) could be firmly embedded in  $\text{g-C}_3\text{N}_4$  and reactive species produced by the interaction of  $\text{H}_2\text{O}_2$  and Cu (I) [81]. The unique adsorption capacity of  $\text{g-C}_3\text{N}_4$  for some organic pollutants also leads to superior degradation performance. Xie et al. investigated that different monochlorophenols isomers (2-chlorophenol, 3-chlorophenol, and 4-chlorophenol) could be degraded efficiently using Co-doped  $\text{g-C}_3\text{N}_4$  as a catalyst in the presence of PMS. It was confirmed that the degradation rate was in the same order as the adsorption quantity [79]. This was attributed to the strong intermolecular forces between pollutant molecules and residual amino groups in the  $\text{g-C}_3\text{N}_4$  fragment [92]. Pd-doped  $\text{g-C}_3\text{N}_4$  was successfully synthesized by anchoring Pd nanoparticles on  $\text{g-C}_3\text{N}_4$  using  $\text{KBH}_4$  reduction method, which was regularly active for PMS activation toward bisphenol A removal [82]. Metal oxide such as manganese oxide [85,90] and iron oxide [68] decorated on  $\text{g-C}_3\text{N}_4$  are also employed for organic pollutions degradation via activating  $\text{H}_2\text{O}_2$  or PMS (Figure 1). Lyu et al. prepared Cu (II)/ $\text{CuAlO}_2/\text{g-C}_3\text{N}_4$  composite as a Fenton-like catalyst. The Cu and C were investigated as dual reaction centers, and C-O-Cu acts as bridges to accelerating electrons transfer [75]. Nonmetal doping is also considered to be an efficient approach to improve electron transfer capability. Electronic structure modulation was achieved in oxygen-doped  $\text{g-C}_3\text{N}_4$  for PMS activation, which was fabricated using urea and oxalic acid dihydrate [66]. The authors further investigated carbon and oxygen doped  $\text{g-C}_3\text{N}_4$  exhibited better PMS activity due to its dual active sites-electron-poor C atoms and electron-rich O atoms [86]. Co-doping of iron and sulfur was found to be an approach to charge distribution and density of  $\text{g-C}_3\text{N}_4$  for PMS activation [83]. To improve its chemical activity and electron transportation ability, Coupling nanocarbon materials  $\text{g-C}_3\text{N}_4$  was developed to realize efficient PMS or  $\text{H}_2\text{O}_2$  activation [87]. Moreover, combining nanocarbon materials and metal doping was frequently fabricated with  $\text{g-C}_3\text{N}_4$  to exploit both materials' synergistic effect [69,77,88].

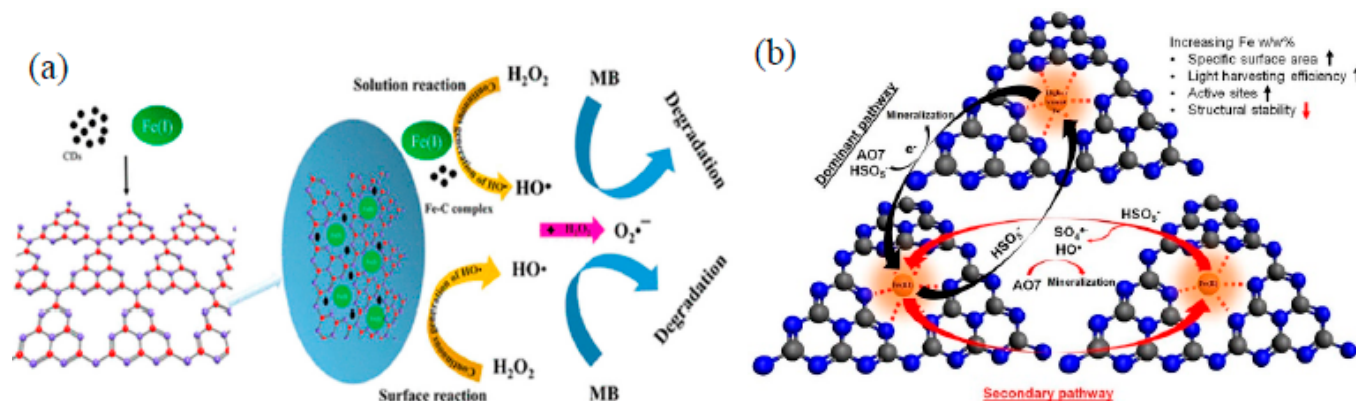


**Figure 1.** (a) Schematic illustration of the catalytic mechanism of  $\text{g-C}_3\text{N}_4/\text{CDs}/\text{Fe(II)}$  in the presence of  $\text{H}_2\text{O}_2$ , reprinted with permission from [68]. Copyright 2019 American Chemical Society. (b) Proposed mechanism of PMS activation by  $\text{gCN-Fe}_3$  for AO7 removal, reprinted with permission from [83]. Copyright 2018 Elsevier.



### 3. Photochemical AOPs

Light irradiation is the most widely used method of applying additional energy to assist reactive species generating, which presents the advantages of simple, clean, relatively inexpensive, and efficient.  $\text{TiO}_2$  and  $\text{ZnO}$  were firstly used as photocatalysts for catalytic oxidation of organic contaminants. In this case, photocatalysis induces the formation of  $\text{h}^+$ ,  $\bullet\text{O}_2^-$  and  $\bullet\text{OH}$ , which act as principle reactive species for pollutants degradation. Consequently, visible light irradiations have been coupled with powerful oxidants such as  $\text{H}_2\text{O}_2$  and PMS, including catalysis with a modified photocatalyst, resulting in various AOPs. In this section, the applications of these different AOPs as photocatalysis, Photo-Fenton (like) reactions, and photo-assisted sulfate radical based AOPs are summarized. Some representative applications of  $\text{g-C}_3\text{N}_4$  based composites as a catalyst in photochemical AOPs are shown in Table 2.

**Table 2.**  $\text{g-C}_3\text{N}_4$  based composites for photochemical AOPs.

Catalyst	Target Contaminants	Light Source	Reaction Conditions	Performance	Ref.
$\text{NiCo}_2\text{O}_4/\text{g-C}_3\text{N}_4$	Carbamazepine	500 W Xenon lamp, Visible light	carbamazepine, 10 mg/L; catalyst, 0.5 g/L; PMS, 1 mM;	100% in 10 min	[93]
$\text{TiO}_2/\text{g-C}_3\text{N}_4$	Acetaminophen	300 W Xenon lamp, Visible light	acetaminophen, 5 mg/L; catalyst, 0.5 g/L; PS, 2 mM; pH, 7	100% in 30 min	[94]
Fe doped $\text{g-C}_3\text{N}_4$ /graphene	Trimethoprim	350 W Xenon lamp, Visible light	Trimethoprim, 0.02 mM; catalyst, 0.5 g/L; PMS, 0.2 mM; pH, 6	100% in 120 min	[95]
$\text{MoS}_2/\text{A g-C}_3\text{N}_4$	Tetracycline	300 W Xenon lamp, Visible light	tetracycline, 20 mg/L; catalyst, 0.2 g/L; PMS, 0.1 mM; T, 20 °C; pH, 5.5	98.9% in 50 min	[96]
activated carbon/ $\text{g-C}_3\text{N}_4$	Atrazine	300 W Xenon lamp, Visible light	atrazine, 5 mg/L; catalyst, 1 g/L; PMS, 5 mM; T, 25 °C; pH, 5.56	97.5% in 120 min	[97]
Cobalt-doped $\text{g-C}_3\text{N}_4$	Rhodamine B	500 W halogen tungsten lamp, Visible light	rhodamine B, 10 mg/L; catalyst, 0.4 g/L; PMS, 0.12 mM; T, 25 °C; pH, 4.68	100% in 25 min	[98]
Sulfur-doped/ $\text{g-C}_3\text{N}_4$	Bisphenol A	150 W Visible light lamp	Bisphenol A, 50 mg/L; catalyst, 0.3 g/L; PMS, 0.3 g/L; T, 20 °C; pH, 5	85% in 120 min	[99]
$\text{g-C}_3\text{N}_4$ -imidazole-based ligand- $\text{FePcCl}_{16}$	Carbamazepine	Xenon lamp, Visible light	carbamazepine, 25 $\mu\text{M}$ ; catalyst, 0.1 g/L; PMS, 0.3 mM; pH, 7	95% in 25 min	[100]
Cu-modified alkalized $\text{g-C}_3\text{N}_4$	Rhodamine B	halogen tungsten lamp, Visible light	rhodamine B, 10 mg/L; catalyst, 0.4 g/L; $\text{H}_2\text{O}_2$ , 9.8 mM; pH, 4.6	95% in 10 min	[101]

#### 3.1. Photocatalysis

As one typical technique of AOPs, photocatalytic degradation held the advantages of non-toxic, convenient operation, and high efficiency. With the irradiation of UV or visible light with energy larger than the semiconductor's energy gap, the electron-donating and electron-accepting sites are formed in the surface of the semiconducting catalyst. The photo-generated electrons migrate from the valence band (VB) to the corresponding conduction band (CB), leaving holes in the VB, resulting in the electrons and holes occupying the CB and VB, respectively. Holes can directly oxidize pollutants or react with  $\text{H}_2\text{O}/\text{OH}^-$  to produce hydroxyl radicals ( $E^\theta_{(\bullet\text{OH}/\text{H}_2\text{O})} = 2.8 \text{ eV/NHE}$ ). Whereas the electrons capture dissolved oxygen ( $\text{O}_2$ ) to yield superoxide radical ( $E^\theta_{(\text{O}_2/\bullet\text{O}_2^-)} = -0.3 \text{ eV/NHE}$ ). The resulting  $\bullet\text{O}_2^-$  are subsequently protonated to produce the  $\bullet\text{OH}$ . Finally, those generated radicals take part in the oxidation of pollutants. In the early seventies, Fujishima and Honda showed the possibility of using the photo-excited semiconductor titanium dioxide ( $\text{TiO}_2$ ) to split water into hydrogen and oxygen in a photo-electrochemical solar cell [102].

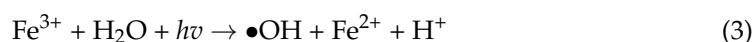
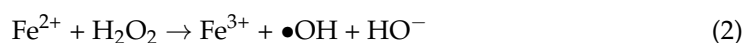
This fundamental work led to developing a new AOP technology, based on semiconductor photocatalysis, for water purification.

g-C<sub>3</sub>N<sub>4</sub> compounds have emerged as up-and-coming candidates to replace TiO<sub>2</sub>, owing to its graphite-like structure and medium bandgap [103,104]. However, the photocatalytic activity of g-C<sub>3</sub>N<sub>4</sub> is still limited by its low electric conductivity and fast recombination of photo-induced carriers [105]. In this regard, modulating the nanostructure of g-C<sub>3</sub>N<sub>4</sub> towards enhancing light harvest efficiency and catalytic mass-transfer is highly desirable. Researchers have made great efforts to design g-C<sub>3</sub>N<sub>4</sub> with various structures, including 3D porous/nanospheres structure, 2D nanosheet and nanorod, etc. [27,37,106]. Such structures such as 3D porous and 2D nanosheet could provide high surface area, exposing more active sites for catalytic surface reactions. Furthermore, nanostructured g-C<sub>3</sub>N<sub>4</sub> could significantly reduce photo-induced carriers' transfer distance, leading to a lower recombination possibility. Moreover, the light quantum efficiencies could be significantly improved by constructing 0D, 1D nanorod, and 2D architectures g-C<sub>3</sub>N<sub>4</sub> [107,108].

The VB top of g-C<sub>3</sub>N<sub>4</sub> locates at about 1.4 V, leading to a small thermo-dynamic force for organic pollutants oxidation. Moreover, the more positive potential of •OH/H<sub>2</sub>O standard redox voltage results the hole cannot directly oxidize the H<sub>2</sub>O to generate •OH ( $E^0(\bullet\text{OH}/\text{H}_2\text{O}) = 2.8 \text{ eV/NHE}$ ). To overcome this shortcoming, several elements of doping have been conducted [44,48,50,108]. Generally, metal doping occurs by inserting into the framework. In contrast, non-metal doping occurs in C or N atoms of g-C<sub>3</sub>N<sub>4</sub> replaced by a heteroatom, which could enhance photocatalytic activity via improve the transfer and separation rates of photogenerated carriers and modulate bandgap [41,47]. Constructing heterojunction is another approach to enhance photodegradation performance for g-C<sub>3</sub>N<sub>4</sub> [109,110]. Generally, Z-schemed heterojunction could be a good option that possesses higher redox potentials in forming reactive radicals and directly hole oxidation ability [111,112].

### 3.2. Photo-Fenton Like Processes

The Photo-Fenton process, the combination of ultraviolet or visible light with the conventional Fenton process, can enhance catalysts' catalytic capacity and increase the degradation efficiency of organic pollutants and reduce iron sludge production [113]. The successive and competitive steps reaction mechanism for the photo-Fenton process are shown in Equations (2) and (3).



As shown in Equation (2), Fe<sup>2+</sup> rapidly reacts with H<sub>2</sub>O<sub>2</sub> to generate Fe<sup>3+</sup>. The main form of Fe<sup>3+</sup> is [Fe(OH)]<sup>2+</sup> at pH 2.8–3.5, which plays a key role in reactions. Subsequently, the reduction of [Fe(OH)]<sup>2+</sup> under light irradiation achieves redox recycling (Figure 2). Moreover, •OH can be generated via direct photolysis of H<sub>2</sub>O<sub>2</sub> [16]. In the photo-Fenton process, the key is to accelerate the reduction of Fe<sup>3+</sup> to Fe<sup>2+</sup> via light irradiation. In the heterogeneous photo-Fenton reactions, the active sites' redox cycle determines the reaction rate [114]. Although g-C<sub>3</sub>N<sub>4</sub> cannot act as active sites for H<sub>2</sub>O<sub>2</sub> decomposition, unique up conversion property, and substantial nitrogen coordinating sites make it become the ideal support for active sites [115]. In addition, the excellent photocatalytic activities of g-C<sub>3</sub>N<sub>4</sub> based composites endue unique advantages as a catalyst for photo-Fenton-like reactions [116]. Metal doping into g-C<sub>3</sub>N<sub>4</sub> is an important approach to enhance degradation efficiency in photo-Fenton reactions. Fe-doped g-C<sub>3</sub>N<sub>4</sub> has been successfully synthesized by thermal shrinkage polymerization for aqueous organic pollutants degradation in photo-Fenton reactions. Introducing Fe in g-C<sub>3</sub>N<sub>4</sub> accelerated the separation of photogenerated electron-holes. The Fe accepts electrons towards rapid reduction from trivalent to divalent, promoting the rapid generation of reactive species [117]. Another report about porous Fe-doped g-C<sub>3</sub>N<sub>4</sub> revealed that the porous g-C<sub>3</sub>N<sub>4</sub> structures enhance the photo-Fenton

activity, owing to more active sites (Fe-N<sub>4</sub>) exposure [118]. An et al. embedded Fe into g-C<sub>3</sub>N<sub>4</sub> by pyrolysis of Fe-N-containing precursor and melamine. The high-density Fe-N<sub>x</sub> was investigated as a reactive site for H<sub>2</sub>O<sub>2</sub> activation [119]. Another strategy used to realize efficient photo-Fenton-based degradation is heterojunction construction, including the Z scheme [120] and type II [121,122]. Zhang et al. prepared MnO<sub>2</sub>/Mn-modified alkalized g-C<sub>3</sub>N<sub>4</sub> by the calcination-impregnating method. It was proposed that Z-scheme charge transfer accelerated the redox cycle of the Mn<sup>4+</sup>/Mn<sup>3+</sup>/Mn<sup>2+</sup> [123].

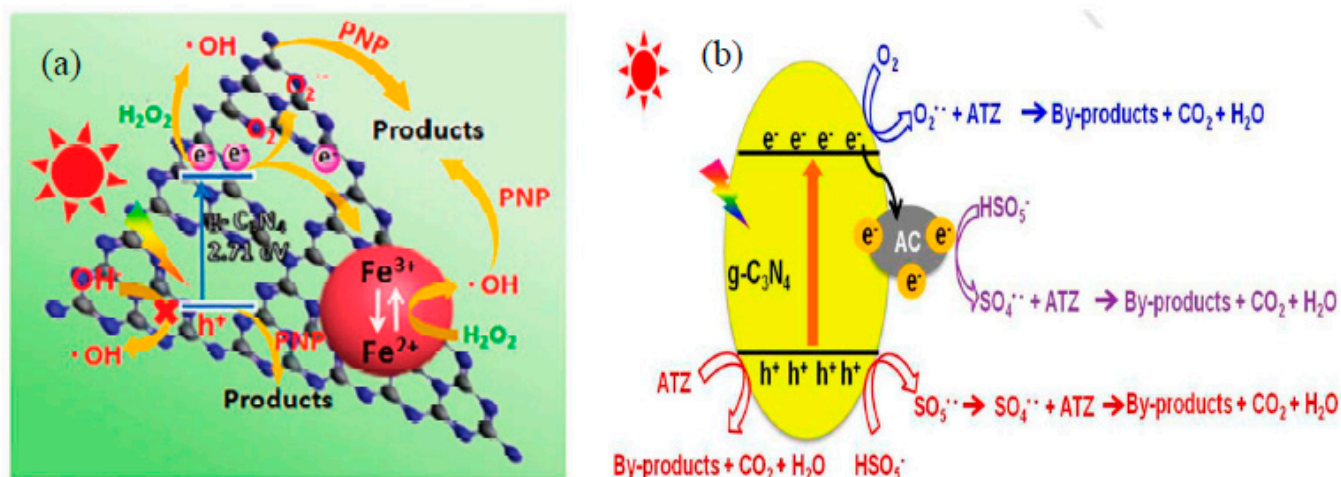
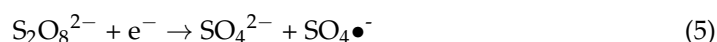
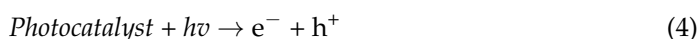


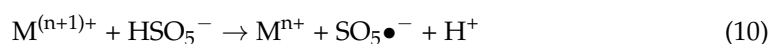
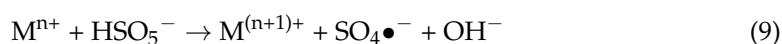
**Figure 2.** (a) schematic illustration of the catalytic mechanism of Fe<sub>2</sub>O<sub>3</sub> QDs/g-C<sub>3</sub>N<sub>4</sub>-900 in H<sub>2</sub>O<sub>2</sub>/vis system, reprinted with permission from [113]. Copyright 2019 John Wiley & Sons, Inc. (b) Mechanism of photocatalytic degradation of atrazine with PMS, reprinted with permission from [96]. Copyright 2018 Elsevier.

### 3.3. Photo-Assisted Sulfate Radical Based AOPs

Sulfate radical-based advanced oxidation processes (SR-AOPs) are increasingly gaining attention as an effective solution to the destruction of recalcitrant organics in water [124]. Among various approaches to generate sulfate radicals via activation of additional sources of reactive species (such as peroxymonosulfate (PMS) and persulfate (PS)), the photo-activation in the presence of a heterogeneous catalyst is worth mentioning [65]. The general mechanism is presented in Equations (4)–(8).



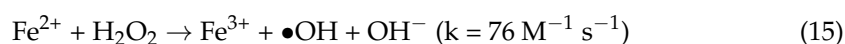
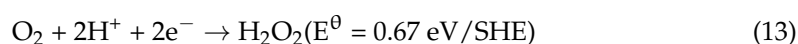
Firstly, photocatalysts are excited under light irradiation to form photo-induced electrons and holes. Then the  $\bullet\text{SO}_4^-$  and  $\bullet\text{OH}$  are generated through the combination of electrons and PMS or PS. When transition metals are constructed into photocatalysts, they could be potential reactive sites for PMS/PS activation (shown in Equations (9)–(12)).



Similar to the application in photo-Fenton-like reactions, g-C<sub>3</sub>N<sub>4</sub> generally plays as reactive site supporters or participate in heterojunction construction in photo-assisted sulfate radical based AOPs. The TiO<sub>2</sub>/g-C<sub>3</sub>N<sub>4</sub> composite was fabricated for paracetamol photocatalytic degradation in the presence of visible light and persulfate. As prepared composite held type II heterojunction, which inhibits the electron-hole recombination in photocatalyst and adding persulfate increased 13 times degradation rate [94]. Liang et al. prepared porous 0D/3D NiCo<sub>2</sub>O<sub>4</sub>/g-C<sub>3</sub>N<sub>4</sub> composite for carbamazepine removal. 99% of degradation was achieved in 10 min under visible light irradiation [93]. Jin et al. constructed Z-scheme MoS<sub>2</sub>/Ag/g-C<sub>3</sub>N<sub>4</sub> via a method of chemical electrostatic adsorption. The deposited Ag further enhances photocatalytic activity via improving light utilization ability and the separation rate of photogenerated e<sup>−</sup>/h<sup>+</sup> pairs. The results indicated that the presence of PMS dramatically accelerates the photocatalytic reaction [96]. Through metal ions such as Fe and Co doping, enhancing photocatalytic activity and improving PMS activation could synchronize implementation towards an efficient organic pollutant removal [95,98].

#### 4. Electrochemical AOPs

Electrochemical advanced oxidation processes (EAOPs) have gained increasing attention as one of the most potent classes of AOP [125–127]. The direct electrochemistry oxidation known as EAOP is anodic oxidation (AO), which is conveniently operated and widely used [125,128]. Electro-Fenton reaction (EF), also known as EAOPs involving the Fenton process, constitutes a clean and effective way to accelerate contaminants degradation via in situ electrocatalytically generated H<sub>2</sub>O<sub>2</sub> from the oxygen reduction reaction (ORR) and regeneration of Fe<sup>2+</sup> on the cathode [126] (Equations (13)–(15)).



One of the EF technology's key points is to fabricate a cathode with high efficiency towards ORR [129,130]. G-C<sub>3</sub>N<sub>4</sub> have been recently considered for cathode modification, which can provide more active sites than other nitrogen-containing materials for electrocatalytic reactions to serve as ORR catalyst. Zhu et al. prepared g-C<sub>3</sub>N<sub>4</sub> doped gas diffusion electrode as a cathode in electro-Fenton processes, and the H<sub>2</sub>O<sub>2</sub> accumulation reached 2.59 mg h<sup>−1</sup> cm<sup>−2</sup>, while it is 1.86 mg h<sup>−1</sup> cm<sup>−2</sup> using cathode without g-C<sub>3</sub>N<sub>4</sub> doping [131]. Loading g-C<sub>3</sub>N<sub>4</sub> on activated carbon fiber electrode was investigated as an efficient way to boost electrocatalytic activity for rhodamine B degradation in electro-Fenton processes, which was due to the g-C<sub>3</sub>N<sub>4</sub> accelerated the cyclic utilization of ferrous ions on the surface of activated carbon fiber [132]. Furthermore, light irradiation was combined with electro-Fenton processes using g-C<sub>3</sub>N<sub>4</sub>/activated carbon fiber and g-C<sub>3</sub>N<sub>4</sub>/carbon nanotube electrodes as cathodes, which achieved higher H<sub>2</sub>O<sub>2</sub> production [133,134]. Moreover, g-C<sub>3</sub>N<sub>4</sub> based composites such as ZnO/g-C<sub>3</sub>N<sub>4</sub> and TiO<sub>2</sub>/g-C<sub>3</sub>N<sub>4</sub> served as photoanodes were applied in photo-assisted anodic oxidation of organic pollution, which was attributed to the superior photocatalytic activity of g-C<sub>3</sub>N<sub>4</sub> [135,136].

#### 5. Conclusions and Perspectives

This review has shown the application of g-C<sub>3</sub>N<sub>4</sub> based composites in various AOPs, including chemical AOPs, photochemical AOPs, and electrochemical AOPs. In the past years, g-C<sub>3</sub>N<sub>4</sub> has been served as an excellent candidate for pollutants removal from water and wastewater thanks to the tunable electronic structure and excellent physicochemical stability. However, pristine g-C<sub>3</sub>N<sub>4</sub> still suffered numerous issues such as smaller surface area, faster recombination of charge, and poor oxidant decomposition activity. It can be summarized the main challenges and strategies in the following aspect:



- (1) For chemicals AOPs, pristine g-C<sub>3</sub>N<sub>4</sub> holds inert activation performance of oxidants such as H<sub>2</sub>O<sub>2</sub> and PMS. Considering that g-C<sub>3</sub>N<sub>4</sub> has excellent affinity to entrap transition metal ions, metal doping is the main strategy to improve the catalytic activity and electrons transfer capability. Combining nanocarbon materials and metal doping was also frequently fabricated with g-C<sub>3</sub>N<sub>4</sub> to exploit both materials' synergistic effect.
- (2) In the case of the photochemical technologies, the challenges for enhancing the photodegradation performance could be ascribed as (1) expand the absorption edge of g-C<sub>3</sub>N<sub>4</sub> and enhance the light-harvesting capability, (2) make separating charge more efficient and suppress the recombination of photo-induced carriers, and (3) coordinate energy band structures to enhance reduction or oxidative capacity. The recent progress of g-C<sub>3</sub>N<sub>4</sub> based composites regarding the photodegradation performance improvement include nanostructure design, element doping, hetero-junction construction, and co-polymerization.
- (3) Cathode modification in electron-Fenton processes is the major application of g-C<sub>3</sub>N<sub>4</sub> based composites in electrochemical AOPs. The key to improving EF performance is to fabricate a cathode with superior ORR efficiency towards higher H<sub>2</sub>O<sub>2</sub> production.

Although g-C<sub>3</sub>N<sub>4</sub> based composite shows promising activity in various AOPs, the synergic effect between different components is still not fully understood. In addition, developing methods towards stable morphology/structure synthesis is highly demanded for practical applications.

**Author Contributions:** Y.S. wrote the paper with the assistance and supervision of A.J.D.s.-G. and M.J.M.d.V. All authors have read and agreed to the published version of the manuscript.

**Funding:** This research was funded by the Spanish Ministerio de Ciencia e Innovación (MICINN) grant number MAT2017-84385-R.

**Institutional Review Board Statement:** "Not applicable" for studies not involving humans or animals.

**Informed Consent Statement:** "Not applicable" for studies not involving humans.

**Acknowledgments:** Yu Shen acknowledges support from the China Scholarship Council (CSC) scholarship (201807040073).

**Conflicts of Interest:** The authors declare no conflict of interest.

## References

1. Krasner, S.W. The Formation and Control of Emerging Disinfection by-Products of Health Concern. *Philos. Trans. R. Soc. A Math. Phys. Eng. Sci.* **2009**, *367*, 4077–4095. [\[CrossRef\]](#)
2. Sauv  , S.; Desrosiers, M. A review of what is an emerging contaminant. *Chem. Central J.* **2014**, *8*, 15. [\[CrossRef\]](#)
3. Oturan, M.A.; Aaron, J.-J. Advanced Oxidation Processes in Water/Wastewater Treatment: Principles and Applications. A Review. *Crit. Rev. Environ. Sci. Technol.* **2014**, *44*, 2577–2641. [\[CrossRef\]](#)
4. Luo, Y.; Guo, W.; Ngo, H.H.; Nghiem, L.D.; Hai, F.I.; Zhang, J.; Liang, S.; Wang, X.C. A review on the occurrence of micropollutants in the aquatic environment and their fate and removal during wastewater treatment. *Sci. Total. Environ.* **2014**, *473–474*, 619–641. [\[CrossRef\]](#)
5. Ternes, T.A.; Meisenheimer, M.; McDowell, D.; Sacher, F.; Brauch, H.-J.; Haist-Gulde, B.; Preuss, G.; Wilme, U.; Zulei-Seibert, N. Removal of Pharmaceuticals During Drinking Water Treatment. *Environ. Sci. Technol.* **2002**, *36*, 3855–3863. [\[CrossRef\]](#)
6. Brown, D.; Laboureur, P. The aerobic biodegradability of primary aromatic amines. *Chemosphere* **1983**, *12*, 405–414. [\[CrossRef\]](#)
7. Rebhun, M.; Meir, A.S.; Laor, Y. Using Dissolved Humic Acid to Remove Hydrophobic Contaminants from Water by Complexation–Flocculation Process. *Environ. Sci. Technol.* **1998**, *32*, 981–986. [\[CrossRef\]](#)
8. Laine, D.F.; Cheng, I.F. The destruction of organic pollutants under mild reaction conditions: A review. *Microchem. J.* **2007**, *85*, 183–193. [\[CrossRef\]](#)
9. Anandan, S.; Ponnusamy, V.K.; AshokKumar, M. A review on hybrid techniques for the degradation of organic pollutants in aqueous environment. *Ultrason. Sonochem.* **2020**, *67*, 105130. [\[CrossRef\]](#) [\[PubMed\]](#)
10. Roberto, A.; Caprio, V.; Insola, A.; Marotta, R. Advanced Oxidation Processes (Aop) for Water Purification and Recovery. *Catal. Today* **1999**, *53*, 51–59.
11. Herrmann, J.M.; Guillard, C.; Arguello, M.; Ag  era, A.; Tejedor, A.; Piedra, L.; Fern  ndez-Alba, A. Photocatalytic Degradation of Pesticide Pirimiphos-Methyl: Determination of the Reaction Pathway and Identification of Intermediate Products by Various Analytical Methods. *Catal. Today* **1999**, *54*, 353–367. [\[CrossRef\]](#)

12. Gogate, P.R.; Pandit, A.B. A review of imperative technologies for wastewater treatment I: Oxidation technologies at ambient conditions. *Adv. Environ. Res.* **2004**, *8*, 501–551. [\[CrossRef\]](#)
13. Gogate, P.R.; Pandit, A.B. A review of imperative technologies for wastewater treatment II: Hybrid methods. *Adv. Environ. Res.* **2004**, *8*, 553–597. [\[CrossRef\]](#)
14. Zhang, M.-H.; Dong, H.; Zhao, L.; Wang, D.-X.; Meng, D. A review on Fenton process for organic wastewater treatment based on optimization perspective. *Sci. Total. Environ.* **2019**, *670*, 110–121. [\[CrossRef\]](#)
15. Dueterberg, C.K.; Mylon, S.E.; Waite, T.D. pH Effects on Iron-Catalyzed Oxidation using Fenton's Reagent. *Environ. Sci. Technol.* **2008**, *42*, 8522–8527. [\[CrossRef\]](#)
16. Pignatello, J.J.; Oliveros, E.; Mackay, A. Advanced Oxidation Processes for Organic Contaminant Destruction Based on the Fenton Reaction and Related Chemistry. *Crit. Rev. Environ. Sci. Technol.* **2006**, *36*, 1–84. [\[CrossRef\]](#)
17. Klavarioti, M.; Mantzavinos, D.; Fatta-Kassinos, D. Removal of residual pharmaceuticals from aqueous systems by advanced oxidation processes. *Environ. Int.* **2009**, *35*, 402–417. [\[CrossRef\]](#)
18. Esplugas, S.; Giménez, J.; Contreras, S.; Pascual, E.; Rodríguez, M. Comparison of different advanced oxidation processes for phenol degradation. *Water Res.* **2002**, *36*, 1034–1042. [\[CrossRef\]](#)
19. Bokare, A.D.; Choi, W. Singlet-Oxygen Generation in Alkaline Periodate Solution. *Environ. Sci. Technol.* **2015**, *49*, 14392–14400. [\[CrossRef\]](#)
20. Ye, T.; Wei, Z.; Spinney, R.; Dionysiou, D.D.; Luo, S.; Chai, L.; Yang, Z.-H.; Xiao, R. Quantitative structure–activity relationship for the apparent rate constants of aromatic contaminants oxidized by ferrate (VI). *Chem. Eng. J.* **2017**, *317*, 258–266. [\[CrossRef\]](#)
21. Trojanowicz, M. Removal of persistent organic pollutants (POPs) from waters and wastewaters by the use of ionizing radiation. *Sci. Total. Environ.* **2020**, *718*, 134425. [\[CrossRef\]](#) [\[PubMed\]](#)
22. Shah, N.S.; Khan, J.A.; Sayed, M.; Khan, Z.U.H.; Iqbal, J.; Arshad, S.; Junaid, M.; Khan, H.M. Synergistic effects of H<sub>2</sub>O<sub>2</sub> and S<sub>2</sub>O<sub>8</sub><sup>2−</sup> in the gamma radiation induced degradation of congo-red dye: Kinetics and toxicities evaluation. *Sep. Purif. Technol.* **2020**, *233*, 115966. [\[CrossRef\]](#)
23. Buthiyappan, A.; Aziz, A.R.A.; Wan, M.A.W.D. Recent Advances and Prospects of Catalytic Advanced Oxidation Process in Treating Textile Effluents. *Rev. Chem. Eng.* **2016**, *32*, 1–47. [\[CrossRef\]](#)
24. Zhu, J.; Xiao, P.; Li, H.; Carabineiro, S.A.C. Graphitic Carbon Nitride: Synthesis, Properties, and Applications in Catalysis. *ACS Appl. Mater. Interfaces* **2014**, *6*, 16449–16465. [\[CrossRef\]](#)
25. Ong, W.-J.; Tan, L.-L.; Ling-Ling, T.; Yong, S.-T.; Chai, S.-P. Graphitic Carbon Nitride (g-C<sub>3</sub>N<sub>4</sub>)-Based Photocatalysts for Artificial Photosynthesis and Environmental Remediation: Are We a Step Closer To Achieving Sustainability? *Chem. Rev.* **2016**, *116*, 7159–7329. [\[CrossRef\]](#)
26. Wang, X.; Maeda, K.; Thomas, A.; Takanabe, K.; Xin, G.; Carlsson, J.M.; Domen, K.; Antonietti, M. A metal-free polymeric photocatalyst for hydrogen production from water under visible light. *Nat. Mater.* **2009**, *8*, 76–80. [\[CrossRef\]](#)
27. Xu, J.; Zhang, L.; Shi, R.; Zhu, Y. Chemical exfoliation of graphitic carbon nitride for efficient heterogeneous photocatalysis. *J. Mater. Chem. A* **2013**, *1*, 14766–14772. [\[CrossRef\]](#)
28. Cui, Y.; Ding, Z.; Liu, P.; Antonietti, M.; Fu, X.; Wang, X. Metal-Free Activation of H<sub>2</sub>O<sub>2</sub> by g-C<sub>3</sub>N<sub>4</sub> under Visible Light Irradiation for the Degradation of Organic Pollutants. *Phys. Chem. Chem. Phys.* **2012**, *14*, 1455–1462. [\[CrossRef\]](#)
29. Liebig, J. Über einige Stickstoff-Verbindungen. *Ann. Pharm.* **1834**, *10*, 1–47. [\[CrossRef\]](#)
30. Goettmann, F.; Fischer, A.; Antonietti, M.; Thomas, A. Metal-free catalysis of sustainable Friedel–Crafts reactions: Direct activation of benzene by carbon nitrides to avoid the use of metal chlorides and halogenated compounds. *Chem. Commun.* **2006**, 4530–4532. [\[CrossRef\]](#)
31. Sudhaik, A.; Raizada, P.; Shandilya, P.; Jeong, D.-Y.; Lim, J.-H.; Singh, P. Review on fabrication of graphitic carbon nitride based efficient nanocomposites for photodegradation of aqueous phase organic pollutants. *J. Ind. Eng. Chem.* **2018**, *67*, 28–51. [\[CrossRef\]](#)
32. Kumar, S.; Karthikeyan, S.; Lee, A.F. g-C<sub>3</sub>N<sub>4</sub>-Based Nanomaterials for Visible Light-Driven Photocatalysis. *Catalysts* **2018**, *8*, 74. [\[CrossRef\]](#)
33. Zhang, S.; Li, J.; Wang, X.; Huang, Y.; Zeng, M.; Xu, J. Rationally Designed 1d Ag@AgVO<sub>3</sub> Nanowire/Graphene/Protonated g-C<sub>3</sub>N<sub>4</sub> Nanosheet Heterojunctions for Enhanced Photocatalysis Via Electrostatic Self-Assembly and Photochemical Reduction Methods. *J. Mater. Chem. A* **2015**, *3*, 10119–10126. [\[CrossRef\]](#)
34. Ye, C.; Li, J.-X.; Li, Z.-J.; Li, X.-B.; Fan, X.-B.; Zhang, L.-P.; Chen, B.; Tung, C.; Wu, L. Enhanced Driving Force and Charge Separation Efficiency of Protonated g-C<sub>3</sub>N<sub>4</sub> for Photocatalytic O<sub>2</sub> Evolution. *ACS Catal.* **2015**, *5*, 6973–6979. [\[CrossRef\]](#)
35. Bai, X.; Wang, L.; Zong, R.; Zhu, Y. Photocatalytic Activity Enhanced via g-C<sub>3</sub>N<sub>4</sub> Nanoplates to Nanorods. *J. Phys. Chem. C* **2013**, *117*, 9952–9961. [\[CrossRef\]](#)
36. Xu, J.; Wang, Y.; Zhu, Y. Nanoporous Graphitic Carbon Nitride with Enhanced Photocatalytic Performance. *Langmuir* **2013**, *29*, 10566–10572. [\[CrossRef\]](#)
37. Zhang, M.; Xu, J.; Zong, R.; Liu, D. Enhancement of visible light photocatalytic activities via porous structure of g-C<sub>3</sub>N<sub>4</sub>. *Appl. Catal. B Environ.* **2014**, *147*, 229–235. [\[CrossRef\]](#)
38. Chen, X.; Zhang, J.; Fu, X.; Antonietti, M.; Wang, X. Fe-g-C<sub>3</sub>N<sub>4</sub>-Catalyzed Oxidation of Benzene to Phenol Using Hydrogen Peroxide and Visible Light. *J. Am. Chem. Soc.* **2009**, *131*, 11658–11659. [\[CrossRef\]](#)
39. Zhang, M.; Bai, X.; Liu, D.; Wang, J.; Liu, D. Enhanced catalytic activity of potassium-doped graphitic carbon nitride induced by lower valence position. *Appl. Catal. B Environ.* **2015**, *164*, 77–81. [\[CrossRef\]](#)

40. Yan, S.; Yan, S.; Wang, J.; Huang, Y.A.; Wang, P.; Li, Z.; Zou, Z. Towards efficient solar hydrogen production by intercalated carbon nitride photocatalyst. *Phys. Chem. Chem. Phys.* **2013**, *15*, 18077–18084. [\[CrossRef\]](#)
41. Wang, X.; Chen, X.; Thomas, A.; Fu, X.; Antonietti, M. Metal-Containing Carbon Nitride Compounds: A New Functional Organic-Metal Hybrid Material. *Adv. Mater.* **2009**, *21*, 1609–1612. [\[CrossRef\]](#)
42. Yan, S.; Yan, S.; Wang, J.; Zou, Z. Ion coordination significantly enhances the photocatalytic activity of graphitic-phase carbon nitride. *Dalton Trans.* **2014**, *43*, 8178–8183. [\[CrossRef\]](#)
43. Hu, S.; Ma, L.; You, J.; Li, F.; Fan, Z.; Lu, G.; Liu, D.; Gui, J. Enhanced visible light photocatalytic performance of g-C<sub>3</sub>N<sub>4</sub> photocatalysts co-doped with iron and phosphorus. *Appl. Surf. Sci.* **2014**, *311*, 164–171. [\[CrossRef\]](#)
44. Pan, H.; Zhang, Y.-W.; Shenoy, V.B.; Gao, H. Ab Initio Study on a Novel Photocatalyst: Functionalized Graphitic Carbon Nitride Nanotube. *ACS Catal.* **2011**, *1*, 99–104. [\[CrossRef\]](#)
45. Liu, G.; Niu, P.; Sun, C.; Smith, S.C.; Chen, Z.; Lu, G.Q.; Cheng, H.-M. Unique Electronic Structure Induced High Photoreactivity of Sulfur-Doped Graphitic C<sub>3</sub>N<sub>4</sub>. *J. Am. Chem. Soc.* **2010**, *132*, 11642–11648. [\[CrossRef\]](#)
46. Zhang, S.; Li, J.; Zeng, M.; Li, J.; Xu, J.; Wang, X. Bandgap Engineering and Mechanism Study of Nonmetal and Metal Ion Codoped Carbon Nitride: C+Fe as an Example. *Chem.-A Eur. J.* **2014**, *20*, 9805–9812. [\[CrossRef\]](#)
47. Ma, X.; Lv, Y.; Xu, J.; Liu, Y.; Zhang, R.; Zhu, Y. A Strategy of Enhancing the Photoactivity of g-C<sub>3</sub>N<sub>4</sub> via Doping of Nonmetal Elements: A First-Principles Study. *J. Phys. Chem. C* **2012**, *116*, 23485–23493. [\[CrossRef\]](#)
48. Zhang, G.; Zhang, M.; Ye, X.; Qiu, X.; Lin, S.; Wang, X. Iodine Modified Carbon Nitride Semiconductors as Visible Light Photocatalysts for Hydrogen Evolution. *Adv. Mater.* **2014**, *26*, 805–809. [\[CrossRef\]](#)
49. Wang, Y.; Di, Y.; Antonietti, M.; Li, H.; Chen, X.; Wang, X. Excellent Visible-Light Photocatalysis of Fluorinated Polymeric Carbon Nitride Solids. *Chem. Mater.* **2010**, *22*, 5119–5121. [\[CrossRef\]](#)
50. Yan, S.C.; Li, Z.S.; Zou, Z.G. Photodegradation of Rhodamine B and Methyl Orange over Boron-Doped g-C<sub>3</sub>N<sub>4</sub> under Visible Light Irradiation. *Langmuir* **2010**, *26*, 3894–3901. [\[CrossRef\]](#)
51. Di, J.; Xia, J.; Xia, J.; Xu, H.; Xu, L.; Xu, Y.; He, M.; Li, H. Preparation of sphere-like g-C<sub>3</sub>N<sub>4</sub>/BiOI photocatalysts via a reactable ionic liquid for visible-light-driven photocatalytic degradation of pollutants. *J. Mater. Chem. A* **2014**, *2*, 5340–5351. [\[CrossRef\]](#)
52. Sui, Y.; Liu, J.; Zhang, Y.; Tian, X.; Chen, W. Dispersed conductive polymer nanoparticles on graphitic carbon nitride for enhanced solar-driven hydrogen evolution from pure water. *Nanoscale* **2013**, *5*, 9150–9155. [\[CrossRef\]](#)
53. He, F.; Chen, G.; Yu, Y.; Hao, S.; Zhou, Y.; Zheng, Y. Facile Approach to Synthesize g-PAN/g-C<sub>3</sub>N<sub>4</sub> Composites with Enhanced Photocatalytic H<sub>2</sub> Evolution Activity. *ACS Appl. Mater. Interfaces* **2014**, *6*, 7171–7179. [\[CrossRef\]](#) [\[PubMed\]](#)
54. Jin, Z.; Murakami, N.; Tsubota, T.; Ohno, T. Complete oxidation of acetaldehyde over a composite photocatalyst of graphitic carbon nitride and tungsten(VI) oxide under visible-light irradiation. *Appl. Catal. B Environ.* **2014**, *150–151*, 479–485. [\[CrossRef\]](#)
55. Sridharan, K.; Jang, E.; Park, T.J. Novel visible light active graphitic C<sub>3</sub>N<sub>4</sub>-TiO<sub>2</sub> composite photocatalyst: Synergistic synthesis, growth and photocatalytic treatment of hazardous pollutants. *Appl. Catal. B Environ.* **2013**, *142–143*, 718–728. [\[CrossRef\]](#)
56. Miranda, C.; Mansilla, H.; Yáñez, J.; Obregón, S.; Colon, G. Improved photocatalytic activity of g-C<sub>3</sub>N<sub>4</sub>/TiO<sub>2</sub> composites prepared by a simple impregnation method. *J. Photochem. Photobiol. A Chem.* **2013**, *253*, 16–21. [\[CrossRef\]](#)
57. Zhou, X.; Jin, B.; Li, L.; Peng, F.; Wang, H.; Yu, H.; Fang, Y. A carbon nitride/TiO<sub>2</sub> nanotube array heterojunction visible-light photocatalyst: Synthesis, characterization, and photoelectrochemical properties. *J. Mater. Chem.* **2012**, *22*, 17900–17905. [\[CrossRef\]](#)
58. Fan, X.; Zhang, L.; Wang, M.; Huang, W.; Zhou, Y.; Li, M.; Cheng, R.; Shi, J. Constructing carbon-nitride-based copolymers via Schiff base chemistry for visible-light photocatalytic hydrogen evolution. *Appl. Catal. B Environ.* **2016**, *182*, 68–73. [\[CrossRef\]](#)
59. Chen, Z.; Pronkin, S.; Feller, T.-P.; Kailasam, K.; Vilé, G.; Albani, D.; Krumeich, F.; Leary, R.; Barnard, J.; Thomas, J.M.; et al. Merging Single-Atom-Dispersed Silver and Carbon Nitride to a Joint Electronic System via Copolymerization with Silver Tricyanomethanide. *ACS Nano* **2016**, *10*, 3166–3175. [\[CrossRef\]](#)
60. Zhang, J.; Chen, X.; Takanebe, K.; Maeda, K.; Domen, K.; Epping, J.D.; Fu, X.; Antonietti, M.; Wang, X. Synthesis of a Carbon Nitride Structure for Visible-Light Catalysis by Copolymerization. *Angew. Chem. Int. Ed.* **2010**, *49*, 441–444. [\[CrossRef\]](#)
61. Zhang, M.; Yao, W.; Lv, Y.; Bai, X.; Liu, Y.; Jiang, W.; Zhu, Y. Enhancement of mineralization ability of C<sub>3</sub>N<sub>4</sub> via a lower valence position by a tetracyanoquinodimethane organic semiconductor. *J. Mater. Chem. A* **2014**, *2*, 11432–11438. [\[CrossRef\]](#)
62. Jin, J.; Sun, K.; Wu, F.; Gao, B.; Wang, Z.; Kang, M.; Bai, Y.; Zhao, Y.; Liu, X.; Xing, B. Single-solute and bi-solute sorption of phenanthrene and dibutyl phthalate by plant- and manure-derived biochars. *Sci. Total. Environ.* **2014**, *473–474*, 308–316. [\[CrossRef\]](#) [\[PubMed\]](#)
63. Han, L.; Ro, K.S.; Sun, K.; Sun, H.; Wang, Z.; Libra, J.A.; Xing, B. New Evidence for High Sorption Capacity of Hydrochar for Hydrophobic Organic Pollutants. *Environ. Sci. Technol.* **2016**, *50*, 13274–13282. [\[CrossRef\]](#) [\[PubMed\]](#)
64. Iervolino, G.; Zammit, I.; Vaiano, V.; Rizzo, L. Limitations and Prospects for Wastewater Treatment by UV and Visible-Light-Active Heterogeneous Photocatalysis: A Critical Review. *Top. Curr. Chem.* **2019**, *378*, 7. [\[CrossRef\]](#) [\[PubMed\]](#)
65. Yang, Q.; Ma, Y.; Chen, F.; Yao, F.; Sun, J.; Wang, S.; Yi, K.; Hou, L.; Li, X.; Wang, D. Recent advances in photo-activated sulfate radical-advanced oxidation process (SR-AOP) for refractory organic pollutants removal in water. *Chem. Eng. J.* **2019**, *378*, 122149. [\[CrossRef\]](#)
66. Gao, Y.; Zhu, Y.; Lyu, L.; Zeng, Q.; Xing, X.; Hu, C. Electronic Structure Modulation of Graphitic Carbon Nitride by Oxygen Doping for Enhanced Catalytic Degradation of Organic Pollutants through Peroxymonosulfate Activation. *Environ. Sci. Technol.* **2018**, *52*, 14371–14380. [\[CrossRef\]](#)



67. Li, H.; Shan, C.; Panab, B. Fe(III)-Doped g-C<sub>3</sub>N<sub>4</sub> Mediated Peroxymonosulfate Activation for Selective Degradation of Phenolic Compounds via High-Valent Iron-Oxo Species. *Environ. Sci. Technol.* **2018**, *52*, 2197–2205. [\[CrossRef\]](#)
68. Ding, Q.; Lam, F.L.; Hu, X. Complete degradation of ciprofloxacin over g-C<sub>3</sub>N<sub>4</sub>-iron oxide composite via heterogeneous dark Fenton reaction. *J. Environ. Manag.* **2019**, *244*, 23–32. [\[CrossRef\]](#)
69. Fang, L.; Liu, Z.; Zhou, C.; Guo, Y.; Feng, Y.; Yang, M. Degradation Mechanism of Methylene Blue by H<sub>2</sub>O<sub>2</sub> and Synthesized Carbon Nanodots/Graphitic Carbon Nitride/Fe(II) Composite. *J. Phys. Chem. C* **2019**, *123*, 26921–26931. [\[CrossRef\]](#)
70. Chen, Z.; Zhang, S.; Liu, Y.; Alharbi, N.S.; Rabah, S.O.; Wang, S.; Wang, X. Synthesis and fabrication of g-C<sub>3</sub>N<sub>4</sub>-based materials and their application in elimination of pollutants. *Sci. Total. Environ.* **2020**, *731*, 139054. [\[CrossRef\]](#)
71. Jiang, W.; Luo, W.; Wang, J.; Zhang, M.; Liu, D. Enhancement of catalytic activity and oxidative ability for graphitic carbon nitride. *J. Photochem. Photobiol. C Photochem. Rev.* **2016**, *28*, 87–115. [\[CrossRef\]](#)
72. Oh, W.-D.; Dong, Z.; Lim, T.-T. Generation of sulfate radical through heterogeneous catalysis for organic contaminants removal: Current development, challenges and prospects. *Appl. Catal. B Environ.* **2016**, *194*, 169–201. [\[CrossRef\]](#)
73. Hu, P.; Long, M. Cobalt-catalyzed sulfate radical-based advanced oxidation: A review on heterogeneous catalysts and applications. *Appl. Catal. B Environ.* **2016**, *181*, 103–117. [\[CrossRef\]](#)
74. Kasprzyk-Hordern, B.; Ziólek, M.; Nawrocki, J. Catalytic ozonation and methods of enhancing molecular ozone reactions in water treatment. *Appl. Catal. B Environ.* **2003**, *46*, 639–669. [\[CrossRef\]](#)
75. Lyu, L.; Yan, D.; Yu, G.; Cao, W.; Hu, C. Efficient Destruction of Pollutants in Water by a Dual-Reaction-Center Fenton-Like Process over Carbon Nitride Compounds-Complexed Cu(II)-CuAlO<sub>2</sub>. *Environ. Sci. Technol.* **2018**, *52*, 4294–4304. [\[CrossRef\]](#)
76. Zhou, C.; Liu, Z.; Fang, L.; Guo, Y.; Feng, Y.; Yang, M. Kinetic and Mechanistic Study of Rhodamine B Degradation by H<sub>2</sub>O<sub>2</sub> and Cu/Al<sub>2</sub>O<sub>3</sub>/g-C<sub>3</sub>N<sub>4</sub> Composite. *Catalysts* **2020**, *10*, 317. [\[CrossRef\]](#)
77. Guo, F.; Lu, J.; Liu, Q.; Zhang, P.; Zhang, A.; Cai, Y.; Wang, Q. Degradation of Acid Orange 7 by peroxymonosulfate activated with the recyclable nanocomposites of g-C<sub>3</sub>N<sub>4</sub> modified magnetic carbon. *Chemosphere* **2018**, *205*, 297–307. [\[CrossRef\]](#)
78. Pi, Y.; Gao, H.; Cao, Y.; Cao, R.; Wang, Y.; Sun, J. Cobalt ferrite supported on carbon nitride matrix prepared using waste battery materials as a peroxymonosulfate activator for the degradation of levofloxacin hydrochloride. *Chem. Eng. J.* **2020**, *379*, 122377. [\[CrossRef\]](#)
79. Xie, M.; Tang, J.; Kong, L.; Lu, W.; Natarajan, V.; Zhu, F.; Zhan, J. Cobalt doped g-C<sub>3</sub>N<sub>4</sub> activation of peroxymonosulfate for monochlorophenols degradation. *Chem. Eng. J.* **2019**, *360*, 1213–1222. [\[CrossRef\]](#)
80. Fan, J.; Qin, H.; Jiang, S. Mn-doped g-C<sub>3</sub>N<sub>4</sub> composite to activate peroxymonosulfate for acetaminophen degradation: The role of superoxide anion and singlet oxygen. *Chem. Eng. J.* **2019**, *359*, 723–732. [\[CrossRef\]](#)
81. Ma, J.; Jia, N.; Shen, C.; Liu, W.; Wen, Y. Stable cuprous active sites in Cu+-graphitic carbon nitride: Structure analysis and performance in Fenton-like reactions. *J. Hazard. Mater.* **2019**, *378*, 120782. [\[CrossRef\]](#) [\[PubMed\]](#)
82. Wang, Y.; Cao, D.; Liu, M.; Zhao, X. Insights into heterogeneous catalytic activation of peroxymonosulfate by Pd/g-C<sub>3</sub>N<sub>4</sub>: The role of superoxide radical and singlet oxygen. *Catal. Commun.* **2017**, *102*, 85–88. [\[CrossRef\]](#)
83. Wang, S.; Liu, Y.; Wang, J. Iron and Sulfur Co-Doped Graphite Carbon Nitride (FeO<sub>y</sub>/S-g-C<sub>3</sub>N<sub>4</sub>) for Activating Peroxymonosulfate to Enhance Sulfamethoxazole Degradation. *Chem. Eng. J.* **2020**, *382*, 122836. [\[CrossRef\]](#)
84. Oh, W.-D.; Ng, C.-Z.; Ng, S.L.; Lim, J.-W.; Leong, K.-H. Rapid degradation of organics by peroxymonosulfate activated with ferric ions embedded in graphitic carbon nitride. *Sep. Purif. Technol.* **2020**, *230*, 115852. [\[CrossRef\]](#)
85. Li, J.; Fang, J.; Gao, L.; Zhang, J.; Ruan, X.; Xu, A.; Li, X. Graphitic carbon nitride induced activity enhancement of OMS-2 catalyst for pollutants degradation with peroxymonosulfate. *Appl. Surf. Sci.* **2017**, *402*, 352–359. [\[CrossRef\]](#)
86. Zhu, Y.; Chen, Z.; Gao, Y.; Hu, C. General synthesis of carbon and oxygen dual-doped graphitic carbon nitride via copolymerization for non-photochemical oxidation of organic pollutant. *J. Hazard. Mater.* **2020**, *394*, 122578. [\[CrossRef\]](#)
87. Wei, M.; Gao, L.; Li, J.; Fang, J.; Cai, W.; Li, X.; Xu, A. Activation of peroxymonosulfate by graphitic carbon nitride loaded on activated carbon for organic pollutants degradation. *J. Hazard. Mater.* **2016**, *316*, 60–68. [\[CrossRef\]](#)
88. Li, H.; Shan, C.; Panab, B. Development of Fe-doped g-C<sub>3</sub>N<sub>4</sub>/graphite mediated peroxymonosulfate activation for degradation of aromatic pollutants via nonradical pathway. *Sci. Total. Environ.* **2019**, *675*, 62–72. [\[CrossRef\]](#)
89. Feng, Y.; Liao, C.-Z.; Kong, L.; Wu, D.; Liu, Y.; Lee, P.-H.; Shih, K. Facile synthesis of highly reactive and stable Fe-doped g-C<sub>3</sub>N<sub>4</sub> composites for peroxymonosulfate activation: A novel nonradical oxidation process. *J. Hazard. Mater.* **2018**, *354*, 63–71. [\[CrossRef\]](#)
90. Chen, C.; Xie, M.; Kong, L.; Lu, W.; Feng, Z.; Zhan, J. Mn<sub>3</sub>O<sub>4</sub> Nanodots Loaded g-C<sub>3</sub>N<sub>4</sub> Nanosheets for Catalytic Membrane Degradation of Organic Contaminants. *J. Hazard. Mater.* **2020**, *390*, 122146. [\[CrossRef\]](#)
91. Oh, W.-D.; Chang, V.W.; Hu, Z.-T.; Goei, R.; Lim, T.-T. Enhancing the catalytic activity of g-C<sub>3</sub>N<sub>4</sub> through Me doping (Me = Cu, Co and Fe) for selective sulfathiazole degradation via redox-based advanced oxidation process. *Chem. Eng. J.* **2017**, *323*, 260–269. [\[CrossRef\]](#)
92. Qin, Z.; Wang, M.; Li, R.; Chen, Y. Novel Cu<sub>3</sub>P/g-C<sub>3</sub>N<sub>4</sub> p-n heterojunction photocatalysts for solar hydrogen generation. *Sci. China Mater.* **2018**, *61*, 861–868. [\[CrossRef\]](#)
93. Jiang, J.; Wang, X.; Zhang, C.; Li, T.; Lin, Y.; Xie, T.; Dong, S. Porous 0D/3D NiCo<sub>2</sub>O<sub>4</sub>/g-C<sub>3</sub>N<sub>4</sub> Accelerate Emerging Pollutant Degradation in PMS/Vis System: Degradation Mechanism, Pathway and Toxicity Assessment. *Chem. Eng. J.* **2020**, *397*, 125356. [\[CrossRef\]](#)
94. Du, X.; Bai, X.; Xu, L.; Yang, L.; Jin, P. Visible-Light Activation of Persulfate by TiO<sub>2</sub>/g-C<sub>3</sub>N<sub>4</sub> Photocatalyst toward Efficient Degradation of Micropollutants. *Chem. Eng. J.* **2020**, *384*, 123245. [\[CrossRef\]](#)



95. Li, R.; Huang, J.; Cai, M.; Huang, J.; Xie, Z.; Zhang, Q.; Liu, Y.; Liu, H.; Lv, W.; Liu, G. Activation of peroxymonosulfate by Fe doped g-C<sub>3</sub>N<sub>4</sub> /graphene under visible light irradiation for Trimethoprim degradation. *J. Hazard. Mater.* **2020**, *384*, 121435. [\[CrossRef\]](#)
96. Jin, C.; Kang, J.; Li, Z.; Wang, M.; Wu, Z.; Xie, Y. Enhanced visible light photocatalytic degradation of tetracycline by MoS<sub>2</sub>/Ag/g-C<sub>3</sub>N<sub>4</sub> Z-scheme composites with peroxymonosulfate. *Appl. Surf. Sci.* **2020**, *514*, 146076. [\[CrossRef\]](#)
97. Dikdim, J.M.D.; Gong, Y.; Noumi, G.B.; Sieliechi, J.M.; Zhao, X.; Ma, N.; Yang, M.; Tchatchueng, J.B. Peroxymonosulfate improved photocatalytic degradation of atrazine by activated carbon/graphitic carbon nitride composite under visible light irradiation. *Chemosphere* **2019**, *217*, 833–842. [\[CrossRef\]](#)
98. Wang, L.; Guo, X.; Chen, Y.; Ai, S.; Ding, H. Cobalt-doped g-C<sub>3</sub>N<sub>4</sub> as a heterogeneous catalyst for photo-assisted activation of peroxymonosulfate for the degradation of organic contaminants. *Appl. Surf. Sci.* **2019**, *467–468*, 954–962. [\[CrossRef\]](#)
99. Lin, K.-Y.A.; Zhang, Z.-Y. Degradation of Bisphenol A using peroxymonosulfate activated by one-step prepared sulfur-doped carbon nitride as a metal-free heterogeneous catalyst. *Chem. Eng. J.* **2017**, *313*, 1320–1327. [\[CrossRef\]](#)
100. Dong, L.; Xu, T.; Chen, W.; Lu, W. Synergistic multiple active species for the photocatalytic degradation of contaminants by imidazole-modified g-C<sub>3</sub>N<sub>4</sub> coordination with iron phthalocyanine in the presence of peroxymonosulfate. *Chem. Eng. J.* **2019**, *357*, 198–208. [\[CrossRef\]](#)
101. Dong, Q.; Chen, Y.; Wang, L.; Ai, S.; Ding, H. Cu-modified alkalized g-C<sub>3</sub>N<sub>4</sub> as photocatalytically assisted heterogeneous Fenton-like catalyst. *Appl. Surf. Sci.* **2017**, *426*, 1133–1140. [\[CrossRef\]](#)
102. Fujishima, A.; Honda, K. Electrochemical Photolysis of Water at a Semiconductor Electrode. *Nature* **1972**, *238*, 37–38. [\[CrossRef\]](#) [\[PubMed\]](#)
103. Kumar, A.; Kumar, A.; Sharma, G.; Ala'a, H.; Naushad, M.; Ghfar, A.A.; Stadler, F.J. Quaternary Magnetic BiOCl/g-C<sub>3</sub>N<sub>4</sub>/Cu<sub>2</sub>O/Fe<sub>3</sub>O<sub>4</sub> Nano-Junction for Visible Light and Solar Powered Degradation of Sulfamethoxazole from Aqueous Environment. *Chem. Eng. J.* **2018**, *334*, 462–478. [\[CrossRef\]](#)
104. Kumar, A.; Sharma, S.K.; Sharma, G.; Naushad, M.; Stadler, F.J. CeO<sub>2</sub>/g-C<sub>3</sub>N<sub>4</sub>/V<sub>2</sub>O<sub>5</sub> Ternary Nano Hetero-Structures Decorated with Cqds for Enhanced Photo-Reduction Capabilities under Different Light Sources: Dual Z-Scheme Mechanism. *J. Alloy. Compd.* **2020**, *838*, 155692. [\[CrossRef\]](#)
105. Tay, Q.; Kanhere, P.D.; Ng, C.F.; Chen, S.; Chakraborty, S.; Huan, A.C.H.; Sum, T.C.; Ahuja, R.; Chen, Z. Defect Engineered g-C<sub>3</sub>N<sub>4</sub> for Efficient Visible Light Photocatalytic Hydrogen Production. *Chem. Mater.* **2015**, *27*, 4930–4933. [\[CrossRef\]](#)
106. Duan, J.; Chen, S.; Jaroniec, M.; Qiao, S.Z. Porous C<sub>3</sub>N<sub>4</sub> Nanolayers@N-Graphene Films as Catalyst Electrodes for Highly Efficient Hydrogen Evolution. *ACS Nano* **2015**, *9*, 931–940. [\[CrossRef\]](#)
107. Zhao, Y.; Zhao, F.; Wang, X.; Xu, C.; Zhang, Z.; Shi, G.; Qu, L. Graphitic Carbon Nitride Nanoribbons: Graphene-Assisted Formation and Synergic Function for Highly Efficient Hydrogen Evolution. *Angew. Chem. Int. Ed.* **2014**, *53*, 13934–13939. [\[CrossRef\]](#)
108. Yu, J.C.; Yu, J.C.; Shen, Z.; Chan, D.K.L.; Gu, T. g-C<sub>3</sub>N<sub>4</sub> quantum dots: Direct synthesis, upconversion properties and photocatalytic application. *Chem. Commun.* **2014**, *50*, 10148–10150. [\[CrossRef\]](#)
109. Iqbal, J.; Shah, N.S.; Sayed, M.; Imran, M.; Muhammad, N.; Howari, F.M.; Alkhoori, S.A.; Khan, J.A.; Khan, Z.U.H.; Bhatnagar, A.; et al. Synergistic effects of activated carbon and nano-zerovalent copper on the performance of hydroxyapatite-alginate beads for the removal of As<sup>3+</sup> from aqueous solution. *J. Clean. Prod.* **2019**, *235*, 875–886. [\[CrossRef\]](#)
110. Kumarab, A.; Kumarib, A.; Sharmaab, G.; Dua, B.; Naushad, M.; Stadler, F.J. Carbon quantum dots and reduced graphene oxide modified self-assembled S@C<sub>3</sub>N<sub>4</sub>/B@C<sub>3</sub>N<sub>4</sub> metal-free nano-photocatalyst for high performance degradation of chloramphenicol. *J. Mol. Liq.* **2020**, *300*, 112356. [\[CrossRef\]](#)
111. Liu, Y.; Wang, R.; Yang, Z.; Du, H.; Jiang, Y.; Shen, C.; Liang, K.; Xu, A.-W. Enhanced visible-light photocatalytic activity of Z-scheme graphitic carbon nitride/oxygen vacancy-rich zinc oxide hybrid photocatalysts. *Chin. J. Catal.* **2015**, *36*, 2135–2144. [\[CrossRef\]](#)
112. Yu, W.; Xu, D.; Peng, T. Enhanced photocatalytic activity of g-C<sub>3</sub>N<sub>4</sub> for selective CO<sub>2</sub> reduction to CH<sub>3</sub>OH via facile coupling of ZnO: A direct Z-scheme mechanism. *J. Mater. Chem. A* **2015**, *3*, 19936–19947. [\[CrossRef\]](#)
113. Hernandez, R.; Zappi, M.E.; Colucci, J.; Jones, R. Comparing the performance of various advanced oxidation processes for treatment of acetone contaminated water. *J. Hazard. Mater.* **2002**, *92*, 33–50. [\[CrossRef\]](#)
114. Xi, J.; Xia, H.; Ning, X.; Zhang, Z.; Liu, J.; Mu, Z.; Zhang, S.; Du, P.; Lu, X. Carbon-Intercalated 0D/2D Hybrid of Hematite Quantum Dots/Graphitic Carbon Nitride Nanosheets as Superior Catalyst for Advanced Oxidation. *Small* **2019**, *15*, e1902744. [\[CrossRef\]](#) [\[PubMed\]](#)
115. Wen, J.; Xie, J.; Chen, X.; Li, X. A review on g-C<sub>3</sub>N<sub>4</sub>-based photocatalysts. *Appl. Surf. Sci.* **2017**, *391*, 72–123. [\[CrossRef\]](#)
116. Mamba, G.; Mishra, A. Graphitic carbon nitride (g-C<sub>3</sub>N<sub>4</sub>) nanocomposites: A new and exciting generation of visible light driven photocatalysts for environmental pollution remediation. *Appl. Catal. B Environ.* **2016**, *198*, 347–377. [\[CrossRef\]](#)
117. Hu, J.; Zhang, P.; An, W.; Liu, L.; Liang, Y.; Cui, W. In-situ Fe-doped g-C<sub>3</sub>N<sub>4</sub> heterogeneous catalyst via photocatalysis-Fenton reaction with enriched photocatalytic performance for removal of complex wastewater. *Appl. Catal. B Environ.* **2019**, *245*, 130–142. [\[CrossRef\]](#)
118. Miao, W.; Liu, Y.; Chen, X.; Zhao, Y.; Mao, S. Tuning layered Fe-doped g-C<sub>3</sub>N<sub>4</sub> structure through pyrolysis for enhanced Fenton and photo-Fenton activities. *Carbon* **2020**, *159*, 461–470. [\[CrossRef\]](#)

119. An, S.; Zhang, G.; Wang, T.; Zhang, W.; Li, K.; Song, C.; Miller, J.T.; Miao, S.; Wang, J.; Guo, X. High-Density Ultra-small Clusters and Single-Atom Fe Sites Embedded in Graphitic Carbon Nitride (g-C<sub>3</sub>N<sub>4</sub>) for Highly Efficient Catalytic Advanced Oxidation Processes. *ACS Nano* **2018**, *12*, 9441–9450. [[CrossRef](#)]
120. Raizada, P.; Khan, A.A.P.; Singh, P. Construction of carbon nanotube mediated Fe doped graphitic carbon nitride and Ag<sub>3</sub>VO<sub>4</sub> based Z-scheme heterojunction for H<sub>2</sub>O<sub>2</sub> assisted 2,4 dimethyl phenol photodegradation. *Sep. Purif. Technol.* **2020**, *247*, 116957. [[CrossRef](#)]
121. Wang, H.; Xu, Y.; Jing, L.; Huang, S.; Li, H.; He, M.; Xu, H.; Li, H. Novel magnetic BaFe<sub>12</sub>O<sub>19</sub>/g-C<sub>3</sub>N<sub>4</sub> composites with enhanced thermocatalytic and photo-Fenton activity under visible-light. *J. Alloy. Compd.* **2017**, *710*, 510–518. [[CrossRef](#)]
122. Yoon, M.; Oh, Y.; Hong, S.; Lee, J.S.; Boppella, R.; Kim, S.H.; Mota, F.M.; Kim, S.O.; Kim, D.H. Synergistically enhanced photocatalytic activity of graphitic carbon nitride and WO<sub>3</sub> nanohybrids mediated by photo-Fenton reaction and H<sub>2</sub>O<sub>2</sub>. *Appl. Catal. B Environ.* **2017**, *206*, 263–270. [[CrossRef](#)]
123. Zhang, Q.; Peng, Y.; Deng, F.; Wang, M.; Chen, D. Porous Z-scheme MnO<sub>2</sub>/Mn-modified Alkalinized g-C<sub>3</sub>N<sub>4</sub> Heterojunction with Excellent Fenton-like Photocatalytic Activity for Efficient Degradation of Pharmaceutical Pollutants. *Sep. Purif. Technol.* **2020**, *246*, 116890. [[CrossRef](#)]
124. Anipsitakis, G.P.; Dionysiou, D.D. Degradation of Organic Contaminants in Water with Sulfate Radicals Generated by the Conjunction of Peroxymonosulfate with Cobalt. *Environ. Sci. Technol.* **2003**, *37*, 4790–4797. [[CrossRef](#)]
125. Martínez-Huitle, C.A.; Ferro, S. Electrochemical oxidation of organic pollutants for the wastewater treatment: Direct and indirect processes. *Chem. Soc. Rev.* **2006**, *35*, 1324–1340. [[CrossRef](#)]
126. Brillas, E.; Sirés, I.; Oturan, M.A. Electro-Fenton Process and Related Electrochemical Technologies Based on Fenton's Reaction Chemistry. *Chem. Rev.* **2009**, *109*, 6570–6631. [[CrossRef](#)]
127. Comninellis, C.; Kapalka, A.; Malato, S.; Parsons, S.A.; Poulios, I.; Mantzavinos, D. Advanced oxidation processes for water treatment: Advances and trends for R&D. *J. Chem. Technol. Biotechnol.* **2008**, *83*, 769–776. [[CrossRef](#)]
128. Panizza, M.; Cerisola, G. Direct and Mediated Anodic Oxidation of Organic Pollutants. *Chem. Rev.* **2009**, *109*, 6541–6569. [[CrossRef](#)]
129. Nidheesh, P.V.; Gandhimathi, R. Removal of Rhodamine B from aqueous solution using graphite–Graphite electro-Fenton system. *Desalin. Water Treat.* **2014**, *52*, 1872–1877. [[CrossRef](#)]
130. Le, T.X.H.; Bechelany, M.; Lacour, S.; Oturan, M.A.; Oturan, M.A.; Cretin, M. High removal efficiency of dye pollutants by electron-Fenton process using a graphene based cathode. *Carbon* **2015**, *94*, 1003–1011. [[CrossRef](#)]
131. Zhu, Y.; Qiu, S.; Deng, F.; Zheng, Y.; Li, K.; Ma, F.; Liang, D. Enhanced degradation of sulfathiazole by electro-Fenton process using a novel carbon nitride modified electrode. *Carbon* **2019**, *145*, 321–332. [[CrossRef](#)]
132. He, Z.; Chen, J.; Chen, Y.; Makwarimba, C.P.; Huang, X.; Zhang, S.; Chen, J.; Song, S. An activated carbon fiber-supported graphite carbon nitride for effective electro-Fenton process. *Electrochim. Acta* **2018**, *276*, 377–388. [[CrossRef](#)]
133. Yu, F.; Wang, Y.; Ma, H.; Chen, Y. Enhancement of H<sub>2</sub>O<sub>2</sub> production and AYR degradation using a synergetic effect of photo-electrocatalysis for carbon nanotube/g-C<sub>3</sub>N<sub>4</sub> electrodes. *New J. Chem.* **2018**, *42*, 16703–16708. [[CrossRef](#)]
134. Yu, F.; Wang, Y.; Ma, H.; Dong, G. Enhancing the yield of hydrogen peroxide and phenol degradation via a synergistic effect of photoelectrocatalysis using a g-C<sub>3</sub>N<sub>4</sub>/ACF electrode. *Int. J. Hydrog. Energy* **2018**, *43*, 19500–19509. [[CrossRef](#)]
135. Wang, J.; Yang, Z.; Gao, X.; Yao, W.; Wei, W.; Chen, X.; Zong, R.; Liu, D. Core-shell g-C<sub>3</sub>N<sub>4</sub>@ZnO composites as photoanodes with double synergistic effects for enhanced visible-light photoelectrocatalytic activities. *Appl. Catal. B Environ.* **2017**, *217*, 169–180. [[CrossRef](#)]
136. Su, Y.; Liu, G.; Zeng, C.; Lu, Y.; Luo, H.; Zhang, R. Carbon Quantum Dots-Decorated TiO<sub>2</sub>/g-C<sub>3</sub>N<sub>4</sub> Film Electrode as a Photoanode with Improved Photoelectrocatalytic Performance for 1,4-Dioxane Degradation. *Chemosphere* **2020**, *251*, 126381. [[CrossRef](#)]